

Experimental Screening and Monte Carlo Simulation of *Psidium guajava* Extract as Green Inhibitor for Carbon Steel Corrosion in the Acidic Environment

A. N. El-hoshoudy ^{1*}, E. G. Zaki ^{1*}, S. M. Elsaheed ¹, and K. M. Zohdy ²

¹ Egyptian Petroleum Research Institute, 11727, Nasr City, Cairo, Egypt

² Higher Technological Institute, 10th of Ramadan City, Cairo, Egypt

Received February 16, 2021; Accepted April 16, 2021

Abstract

The effectiveness of corrosive inhibition for carbon steel in acidic media 0.5 M HCl through *Psidium guajava* extract was explored using potentiodynamic polarization (PDP) and Electrochemical Impedance Spectroscopy (EIS). The acquired results indicate that *Psidium guajava* (PG) has good corrosion inhibition performance associated with the increase of *Psidium guajava* concentration over the range of 10 to 100 ppm. The inhibition performance of the *Psidium guajava* was due to the adsorption of heteroatoms (O and N) of *Psidium guajava* on the metallic outer layer, that give rise to the creation of a physisorption protective outlier with lower permeability and enhanced resistance of charge transfer. The corrosion inhibition outputs designated the prospective use of *Psidium guajava* as an effective corrosion inhibitor, especially in the oil-gas industry. Furthermore, computational chemistry tools were conducted to evaluate the electronic geometries, and the adsorption capacity of the screened compounds based on Monte Carlo simulation and the density functional theory (DFT).

Keywords: *Psidium guajava*; Green chemistry; Corrosion inhibition; DFT theory; Monte Carlo (MC) simulation.

1. Introduction

Corrosion inhibition in the acidic environment against acidic consumption and metallic dissolution performed by the usage of different inhibiting agents [1-2]. The well-recognized harmful impact of most corrosion inhibitors has inspired researchers to utilize inexpensive, and renewable natural products as corrosion inhibitor agents. The natural sources are environmentally, and ecologically acceptable products that can be derived from the surrounding ecological systems. Botanical extracts contain many biodegradable compounds. Many plants leave extracts have been investigated for the corrosive inhibition of mild steel in acidic media as reported elsewhere [3-8]. Owing to the wide application of steel in different technological industries, so its protection against acid corrosive action is a critical task [9]. In the current study, theoretical and semi-empirical approaches are implemented to assess the corrosion inhibition efficiencies of different chemical structures. Consequently, the quantum chemical parameters are a powerful tool in the estimation of corrosive inhibition effectiveness through correlating the inhibition effectiveness to the compound's molecular properties which adjust the adsorption tendency on the metallic surface [10-12]. Computational chemistry is a significant tool to screen chemical and quantum factors based on theoretical approaches [10,13-16]. Molecular dynamics (MD) simulation provide a reliable concept about the alignment of corrosive inhibitors over the metal surfaces [17]. A density functional theory (DFT) approach estimates the inhibition effect of organic compounds through their electronic molecular structure [9-10]. Previous publications investigated the efficiency of corrosion inhibition through computational chemistry tools. In this regard, Wang *et al.* [18] apply the DFT approach through the B3LYP/6-31G(d) level to investigate the inhibition efficiency of bipyrazolic- compounds through various chemical descriptors. Musa *et al.* [12] apply a molecular dynamics approach to assess the inhibition efficiency of phthalazone, phthalazine, and phthalhydrazide, on mild iron in acidic media of 1.0 M HCl at 30°C. Gad and Al-Fahemi [19] use chemical descriptors calculated from

DFT theory to study corrosive inhibition efficiency of 2-(alkyloxy)-N,N,N-tris(2-hydroxyethyl)-2-oxoethanaminium chloride (where R= C₆, C₁₂, and C₁₈) on carbon steel (Type L-52) in H₂SO₄ solution (0.5 M). Al-Fahemi *et al.* [20] investigate the corrosion inhibition of melatonin drugs on the surface of carbon steel in H₂SO₄ solution (0.5 M) using the DFT approach and quantum chemical descriptors. Kaya *et al.* [21] use tools of quantum chemistry and molecular dynamic simulation to evaluate corrosion inhibition performance of aspartate, lysine, alanine, asparagine, methionine, histidine, and arginine amino acids on Cu (111)/50 H₂O interfaces. Gad *et al.* [22] assess the corrosive inhibition effect of 4-mercaptop-1-alkylpyridin-1-ium bromide on carbon steel in 1.0 M HCl solution using the DFT approach. Verma *et al.* [23] used the DFT approach to investigate the corrosive dissolution of mild steel using the leaf extract of *Holoptelea integrifolia* in 1.0 M HCl solution. Abdallah *et al.* [24] investigated the theoretical concept of azole compounds as a corrosive inhibitor on an aluminum surface using DFT theory. Negm *et al.* [11] investigated the inhibition efficiencies of three tricationic surfactants synthesized by the quaternization of pentamethyl diethylenetriamine. Dagdag *et al.* [17] investigated the inhibition efficiencies on carbon steel using epoxy resins in 1.0 M HCl medium through global computational parameters. Moreover, they screened adsorption behavior on a metallic surface through Monte Carlo (MC) simulations. Obot *et al.* [9] implement DFT theory at the B₃LYP/6-311⁺⁺G (d,p) level to screen corrosion inhibition of different alkyl carboxylates on X60 steel in 0.5 M HCl solution. Bedair *et al.* [25] apply Monte Carlo simulations and density functional approach (DFT) to investigate corrosive inhibition of new Schiff base compounds on steel surface in 1.0 M HCl. In the current study, quantum chemical computations obeying the DFT theory at the B3LYP level is conducted to hypothetically clarify the inhibitor-steel corrosion inhibition on the molecular and atomic levels [9,18-19]. This study comprises four structures extracted from *Psidium guajava* extract as summarized in Scheme 1. The chemical descriptors including chemical hardness, chemical potential, electronegativity, electrophilicity, and nucleophilicity have been implemented in this study for investigating the compatibility between theoretical and experimental data [21]. These descriptors will characterize the compounds depending on the molecular geometry and define inhibition mechanism of compounds in terms of their chemical reactivity [11]. Moreover, MC simulations were conducted to investigate adsorption energies on the surface of iron (Fe) crystal [12]. Although the Guajava extracts contains tenths of compounds, the theoretical modeling and Monte Carlo simulations were conducted on four compounds or inhibitors only as they are the most efficient components as corrosion inhibitors. The new contribution of this manuscript can be summarized in the following aspects; i) Special carbon steel were implemented [C(0.22), S(0.03), P(0.03), Mn(0.9)], and Fe (balance) detected by X-ray fluorescence, ii) Cheap, ease and green method for inhibitor extraction were conducted, and iii) The inhibitor gives high efficiency with low concentration (100 ppm gives 98 % efficiency) as compared to the results stated by Anupama and Abraham; and Victoria *et al.*, [26-27] which reported that 10 mL of inhibitor gives 66 % efficiency, and 1200 ppm of inhibitor give 74 % efficiency respectively.

2. Materials and reagents

2.1. Plant extract preparation

Fresh leaves of the *Psidium guajava* plant was collected from the region of Shebin El-Kom City, Menofia, Egypt. The plant selected according to its high content of flavonoids, and alkaloids structures as shown in Scheme 1. The collected plant material (~ 2.0 kg) washed thoroughly with deionized water, air-dried in darkness at 25°C. After that, 20.0 g of the leaves were extracted by soaking with 70% ethanol/water (100 cc). The extraction process was performed at 25 °C for seven days, then the extract filtrated, vacuum dried, and stored at 4°C for additional experiments.

2.2. Preparation of solutions

1000 ppm stock solution of *Psidium guajava* prepared by dissolving 1.0 gm of plant extract in 200 mL 70% methanol/water till complete dissolution, add 800 ml distillate, and kept for

use. The screened carbon steel hampered into a Teflon jacket with 1.0 cm^2 uncovered surface area. The chemical analysis (wt %) of carbon steel (CS) were found to be C(0.22), S(0.03), Mn(0.9), P(0.03), and Fe (Balance) detected by X-ray fluorescence. The carbon steel was polished by SiC abrasive papers (320, 500, 800, and 1200 grit) respectively, then subjected to ethyl alcohol (99%) and acetone, dried at 25°C , and stored in a desiccator before usage.

IUPAC name	Molecular Formula	Abbreviation	Molecular structure
2-(3,4-dihydroxyphenyl)-5,7-dihydroxy-3-(((2R,3R,4S,5R)-3,4,5-trihydroxytetrahydro-2H-pyran-2-yl)oxy)-4H-chromen-4-one	$\text{C}_{20}\text{H}_{18}\text{O}_{11}$	C_{20}	
4-hydroxyphenethyl palmitate	$\text{C}_{24}\text{H}_{40}\text{O}_3$	C_{24}	
2,4,6-trihydroxy-5-((1S)-((1R,4R,6R)-6-(2-hydroxypropan-2-yl)-4-methyl-1,2,3,4,6,7,8,8a-octahydronaphthalen-1-yl)(phenyl)methyl)isophthalaldehyde	$\text{C}_{29}\text{H}_{34}\text{O}_6$	C_{29}	
(1aR,7aR,8R,13bS,Z)-9,11-dihydroxy-1,1,4,7a-tetramethyl-8-phenyl-1,1a,2,3,6,7,7a,8,13a,13b-decahydrocyclopropa[9,10]cyclodeca[1,2-b]chromene-10,12-dicarbaldehyde	$\text{C}_{30}\text{H}_{34}\text{O}_5$	C_{30}	

Scheme 1. The molecular structure of the reported Guajava extract compounds

2.3. Solutions

The solutions of *Psidium guajava* inhibitors were prepared in an acidic solution of 0.5 M HCl. The corrosion runs were tested in 0.5 M HCl in the presence and absence of different concentrations (10-100 ppm) of *Psidium guajava*. In each run, a fresh solution is used under an atmospheric condition without agitation.

2.4. Electrochemical experiments

Electrochemical evaluations were accomplished by electrochemical methods, Gamry PCI300/4 Potentiostat/Galvanostat/Zra analyzer, connected with a controllable program. Echem Analyst programming was utilized for every investigation. Utilizing a run of the mill three-cathode cell framework to continue with the potentiodynamic analyses and EIS estimations at 298 K, (i.e. the reference electrode was calomel cathode (SCE), working anode was the example gathered with the carbon steel, and the counter anode was platinum anode (CE). Concerning electrochemical impedance spectroscopy (EIS) estimations, the excitation signal adequacy is 5 mV and the scope of recurrence is 100 kHz to 0.01 Hz at the open circuit potential (OCP) of 1800 s to achieve a steady-state. The used method naturally selects the information that exists in the Tafel plots (± 250 mV as for the consumption potential). The electrochemical Analyses ascertains the corrosion current thickness, consumption potential, anodic and cathodic plots. The scan rate is 2 mVs^{-1} , with a potential region of ± 250 mV dependent on the OCP,. Other than, all investigations were done multiple instances to assure preliminary reproducibility.

3. Results and discussion

3.1. Electrochemical impedance spectroscopy

The corrosion performance of carbon steel through the formation water in the presence and absence of several concentrations of guajava (GU) extract was exhibited via EIS technique [25].

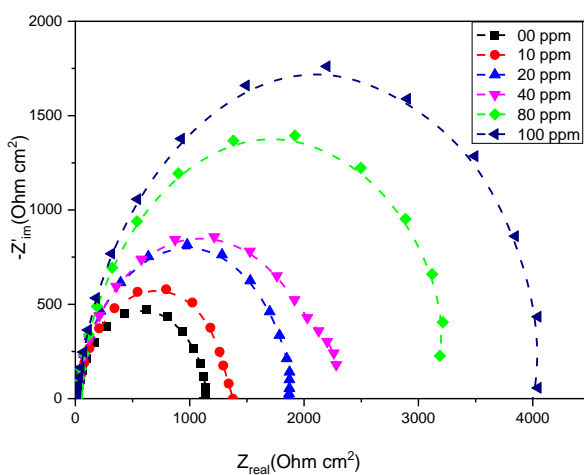


Figure 1. Nyquist impedance curves in 0.5 M HCl of various GU concentrations at different temperatures

These examinations were directed to show the dynamics between the carbon steel and acidic arrangement at various concentrations. Figure 1 shows Nyquist impedance plots for the CS in 0.5 M HCl at 298 K through guajava extract. As displayed in Figure 1, the CS shows a half-circle that its width got greater with the expansion of the inhibitor concentration. Also, the growth of inhibitor concentration raises the interface impedance $|Z|$. This performance shows that the rise of inhibitor concentration lowers the steel dissolution in 0.5 M HCl medium through enhancing its consumption/obstruction. The obtained results are illustrated in Table 1.

Table 1. Electrochemical factors of impedance for carbon steel immersed in 0.5 M HCl in the presence and absence of various concentrations GU

	00 ppm	10 ppm	20 ppm	40 ppm	80 ppm	100 ppm
R _p , ohms	1124	1365	1628	1874	3375	4132
R _u , ohms	14.9	16.1	10.5	10.4	10.1	10.5
CF _{dl}	0.00003735	0.00001982	0.00004189	0.00004139	0.00003859	0.00004098

The CS impedance data were examined and fitted to a simple equivalent circuit as displayed in Figure 2. It consists of a parallel combination of a resistor (R_p , correspond to the resistance of polarization), and a capacitor (C_{dl} , correspond to the interface double layer capacity) in a series with the solution resistance component (R_s). The circuit impedance (Z), is associated with the a.c. signal frequency (f), R_p , and R_s [28-30].

$$Z = R_s + [R_p / (1 + (j2\pi f C_{dl} R_p))] \quad (1)$$

where α measures the deviancy range from the ideal RC-performance of the electrode/electrolyte interface ($0 \leq \alpha \leq 1$).

Equation 1 is a Cole-Cole frequency distribution utilized to define the low rounded curves occurrence. Iron corrosion in acidic media alters the surface inhomogeneous and rough. So, the capacitance is presented through a constant phase element (CPE). The calculated equivalent circuit parameters are summarized in Table 2. The efficiency of the extract was computed using the following formula.

$$IE\% = [1 - (R_p^{(b)} / R_p^{(in)})] \times 100 \quad (2)$$

where $R_p^{(b)}$ and $R_p^{(in)}$ are the resistance of polarization in the presence and absence of the GU, respectively.

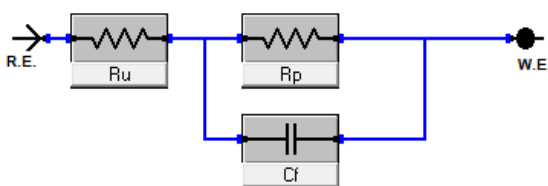
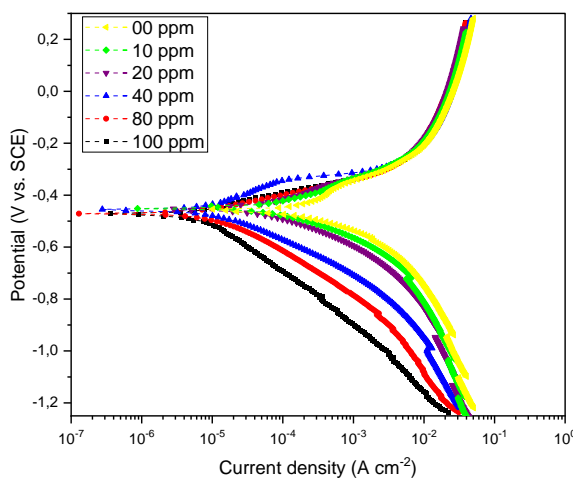


Figure 2. The equivalent circuit model used to fit the EIS outputs for the CS in the presence and absence of (gu) in 0.5 M HCl solution at 298 K

Table 1 summarizes the efficiency% achieved under several circumstances. The electrochemical impedance spectroscopy outputs were attuned to suitable the equivalent circuit as displayed in Figure 2 using Echem Analyst software and the gained related details are summarized in Table 2. This equivalent circuit model was used to fit the added electrochemical impedance spectroscopy to evaluate corrosive inhibition of CS in 0.5 M HCl [31].

3.2. Electrochemical polarization measurements



That energy from anodic/cathodic responses throughout corrosion procedure could be investigated by polarization investigations [32]. The impact for Gu mixes on the polarization from CS in 0.5 M HCl needs to be considered. From Figure 3, it may be apparent starting with the particular polarization curves that increasing GU concentration, decreases the corrosion rate as indicated in Table 2.

Figure 3. Polarization curves for CS immersed in 0.5 M HCl in the presence and absence of various GU concentrations

Table 2. Electrochemical kinetic factors result from CS potentiodynamic polarization measurements immersed in 0.5 M HCl acid in the presence and absence of different GU concentrations

Electrode	Ecorr. mV	Icorr. μA/cm²	Tafel slopes		Corrosion rate (C.R.) mpy	IE %	Θ
			β_a V/decade	β_c V/decade			
00 ppm	-456	579	0.331	0.274	106.6	0	0.000
10 ppm	-433	82	0.274	0.168	47.28	86	0.858
20 ppm	-456	54	0.199	0.228	31.15	91	0.907
40 ppm	-454	40	0.184	0.211	24.55	93	0.931
80 ppm	-471	21.6	0.141	0.212	12.46	96	0.963
100 ppm	-473	9.97	0.132	0.215	5.75	98	0.983

$$EF = 1 - \frac{I_{corr}^0}{R_{corr}} \quad (3)$$

Those cathodic curves were moved with even more negative possibilities. This can be anticipated from the inhibitor adsorption over the metal surface [33]. Electrochemical corrosion dynamic parameters (E_{corr} versus SCE), cathodic and anodic Tafel plots (β_c and β_a), and corrosion current (I_{corr}), were obtained by the framework for Tafel extrapolation towards E_{corr} values. The corrosion efficiency calculated from I_{corr} using equation 3 [34] as summarized in Table 3. R_{corr} and I_{corr} signify corrosive thickness in the absence of inhibitors. Furthermore, corrosion thickness declines regularly by increasing inhibitor concentrations. The anodic and cathodic response from metal dissolution and hydrogen advancement respectively were decelerated. These observations confirm that the inhibitor performs a blended kind of cathodic disposition [35]. The transforms for both Tafel slopes examining the introduction of inhibitor under the hostility medium resort to the concentration of the blended kind inhibitor.

$$Rp = \frac{\beta_a \beta_c}{2.303 * (\beta_a + \beta_c)} \times \frac{1}{I_{corr}} \quad (4)$$

Those comparative control efficiency obtained from each one of the inspected techniques reveals the striking inhibition efficiency of the guajava (GU) extract.

3.3. Temperature effect

The impact of temperature on the consumption rate of the CS in 0.5 M HCl includes 100 ppm of GU was investigated. Figures 4 & 5 displayed the impact of temperature on %IE at various dosages of the compound for CS disintegration in 0.5 M HCl medium at various temperatures. By raising the temperature, the IE% rises as shown in Tables 3 & 4, demonstrating that the adsorption of the inhibitor on the CS surface is mixed [36].

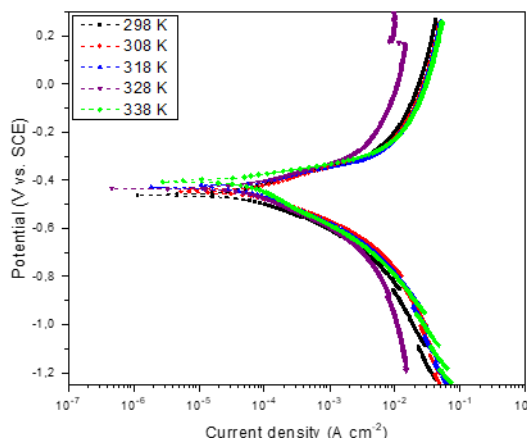


Figure 4. Polarization curves for CS immersed in 0.5 M HCl solution at 100 ppm of GU at different temperatures

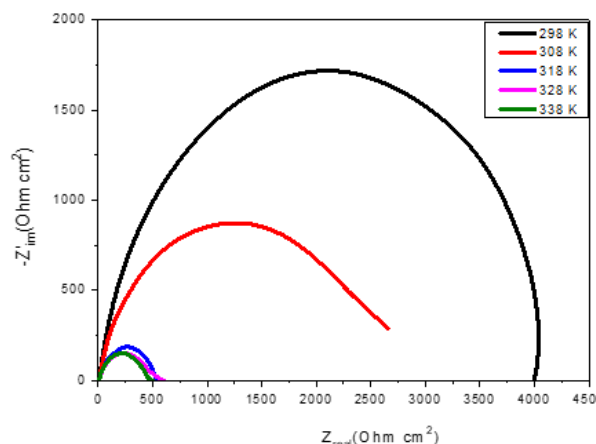


Figure 5. Nyquist impedance curves for CS immersed in 0.5 M HCl solution at 100 ppm of GU at different temperatures

Table 3: Electrochemical kinetic factors result from potentiodynamic polarization of CS immersed in 0.5 M HCl at 100 ppm of GU in the presence and absence of different concentrations of Guajava at various temperatures.

Electrode	E_{corr} mV	I_{corr} μA/cm²	Tafel slopes		Corrosion rate (C.R.) mpy
			β_a V/decade	β_c V/decade	
298 K	-473	9.97	0.132	0.215	5.75
308 K	-433	82	0.215	0.168	47.28
318 K	-462	112	0.185	0.177	64.84
328 K	-433	134	0.175	0.185	77.52
338 K	-446	158	0.207	0.199	90.87

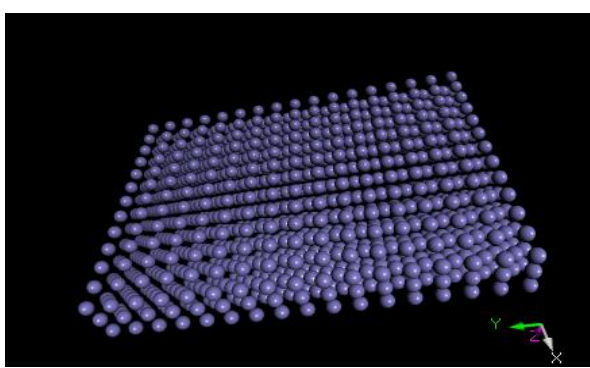
Table 4. Electrochemical parameters of impedance for CS immersed in 0.5 M HCl at 100 ppm of GU IN the presence and absence of different Guajava concentrations at various temperatures

100 ppm	298 K	308 K	318 K	328 K	338 K
R _p ohms	4132	2493	537	490	301
R _u ohms	10.5	9.9	10.5	7.6	7.8
C _f F	0.00004098	0.00003841	0.00003271	0.00003272	0.00003197

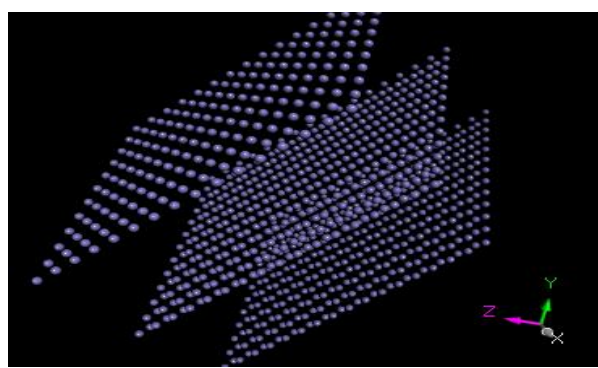
4. Computational calculations

4.1. Monte Carlo simulation

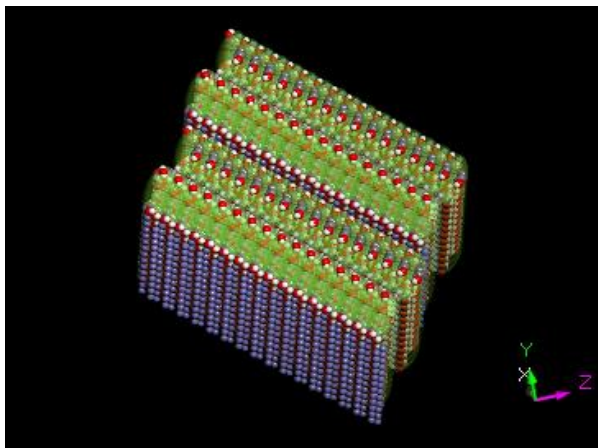
Molecular dynamics approach conducted with the Metropolis Monte Carlo (MC) simulations implemented in *DS-BIOVIA Materials Studio 2017* to inspect the orientation and adsorption performance of the reported inhibitors on the surface of iron metal [37]. The MC computation was optimized to calculate the lowest configuration adsorption energies between the inhibitor molecules and iron metal in the aqueous phase. Firstly, inhibitor molecules were geometry optimized through the Forcite module applying the universal force field [12]. Fe crystal built with a surface cleavage of (111) and vacuum slab of 25.00 Å thickness optimized for the simulation. The interaction conducted in a simulation box (4.05 °A × 4.05 °A × 25.82 °A) with periodic boundary conditions built by using the Crystal Builder [25]. The annealing simulation was conducted in a simulation box contain the reported inhibitor molecules, 50 water molecules on the surface of Fe (111) crystal through Adsorption Locator Module [21] with the same force field (universal) [17]. During the simulation course, the adsorbed inhibitors rotated randomly and translated around the metal surface to find minimum adsorption energy sites [12]. A sequence of NVT (canonical ensemble) calculations were performed with a time step of 0.5 fs at 1 atm and 300 K [17]. The configurations obtained through the annealing simulation as illustrated in Figure 6a-j. The Forcite module is a classical molecular mechanics module that permits rapid energy computations, consistent and periodic geometry optimization of molecules [12]. The Adsorption locator module “distinguishes available adsorption configurations through Monte Carlo computations (simulated annealing) of the configurational space through the metal-adsorbate structure as the temperature is gradually reduced [12]. The MC calculation outputs in the case of four inhibitors on Fe (111) surface including Van der Waals energy, electrostatic energy, the total energy, average total energy, energy distribution, and intermolecular energies as well as the calculation inputs are supplied in the supporting information (Figures S1-S2 and Tables S2-S5).



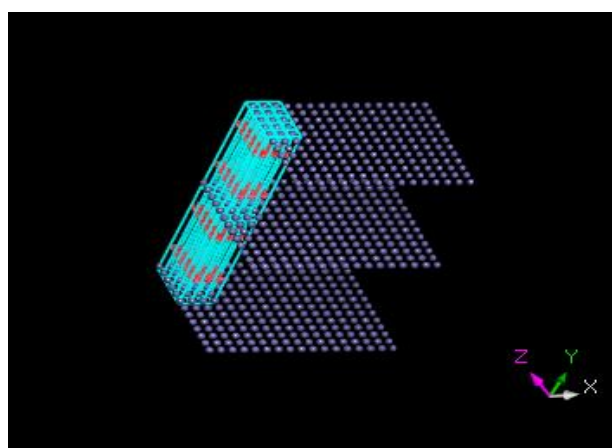
(a) Fe crystal



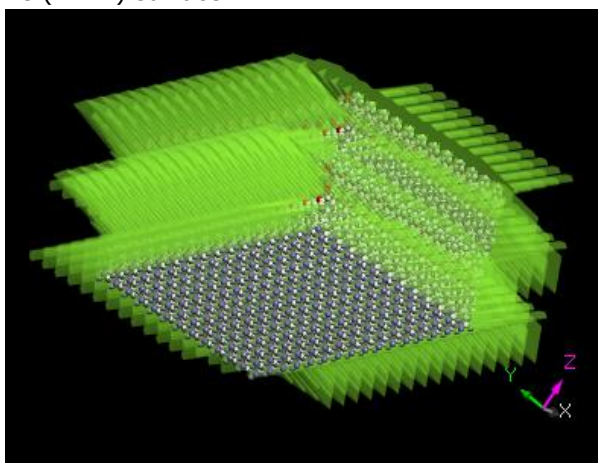
(b) the surface of Fe (111) vacuum slab crystal



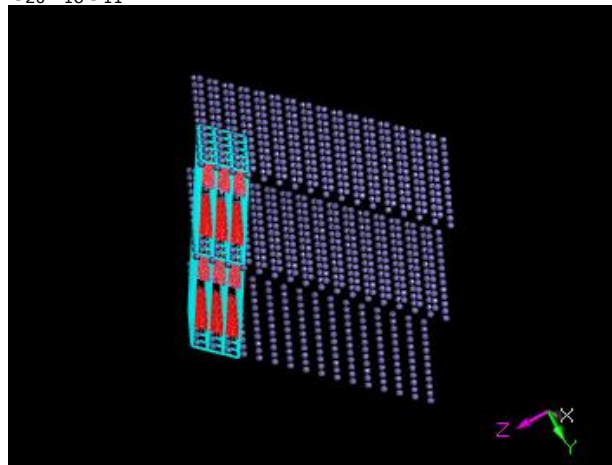
(c) Adsorption annealing of $C_{20}H_{18}O_{11}$ on Fe (1 1 1) surface



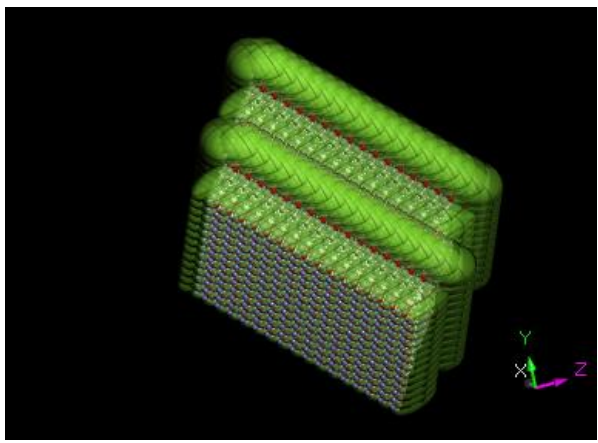
(d) Fe (1 1 1) adsorption annealing fields of $C_{20}H_{18}O_{11}$



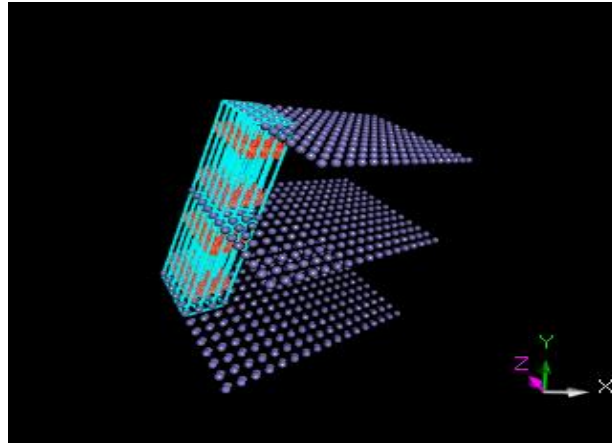
(e) Adsorption annealing of $C_{24}H_{40}O_3$ on Fe (1 1 1) surface



(f) Fe (1 1 1) adsorption annealing fields of $C_{24}H_{40}O_3$



(g) Adsorption annealing of $C_{29}H_{34}O_6$ on Fe (1 1 1) surface



(h) Fe (1 1 1) adsorption annealing fields of $C_{29}H_{34}O_6$

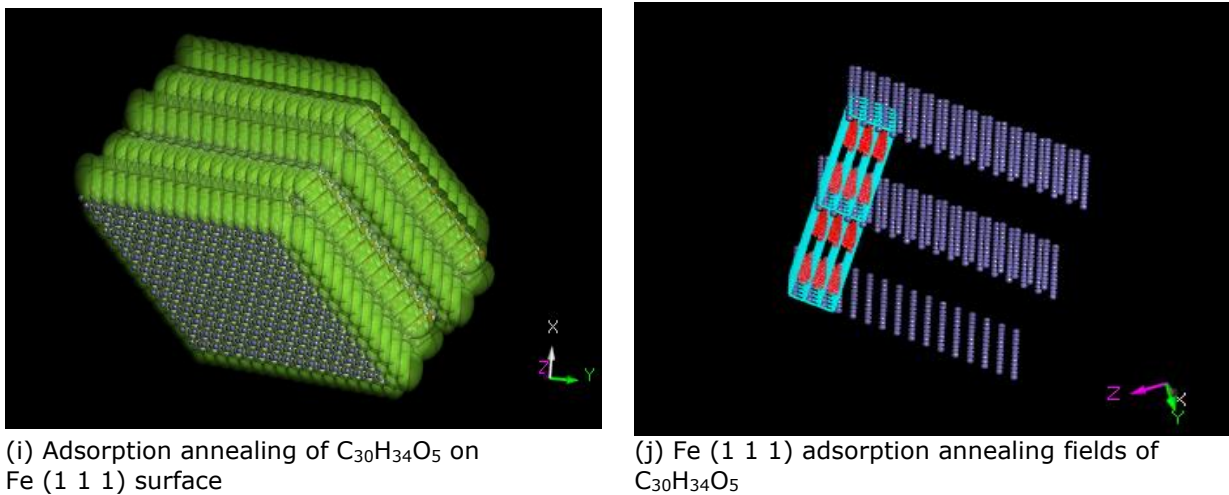


Figure 6. Configurations obtained by MC annealing simulation of the adsorption of the reported inhibitors on Fe (111) surface

The chemical descriptors computed by the MC simulation are summarized in supporting information (Table S5). Since, the adsorption energies provide a powerful tool to evaluate the inhibitor efficiency, where high adsorption energy reveals a more stable configuration and stronger adsorption interaction [21]. A comparison of adsorption energy at each simulation step on the surface of Fe (111) crystal is illustrated in Figure 7. From Table 5 and Figure 7, the average adsorption energies of the reported inhibitors increased in the order of $C_{20}H_{18}O_{11}$ < $C_{29}H_{34}O_6$ < $C_{30}H_{34}O_5$ < $C_{24}H_{40}O_3$, where $C_{24}H_{40}O_3$ give the maximum adsorption energy. Consequently, $C_{24}H_{40}O_3$ performs greater inhibition efficiency as compared to other inhibitor molecules [12,17,38-39].

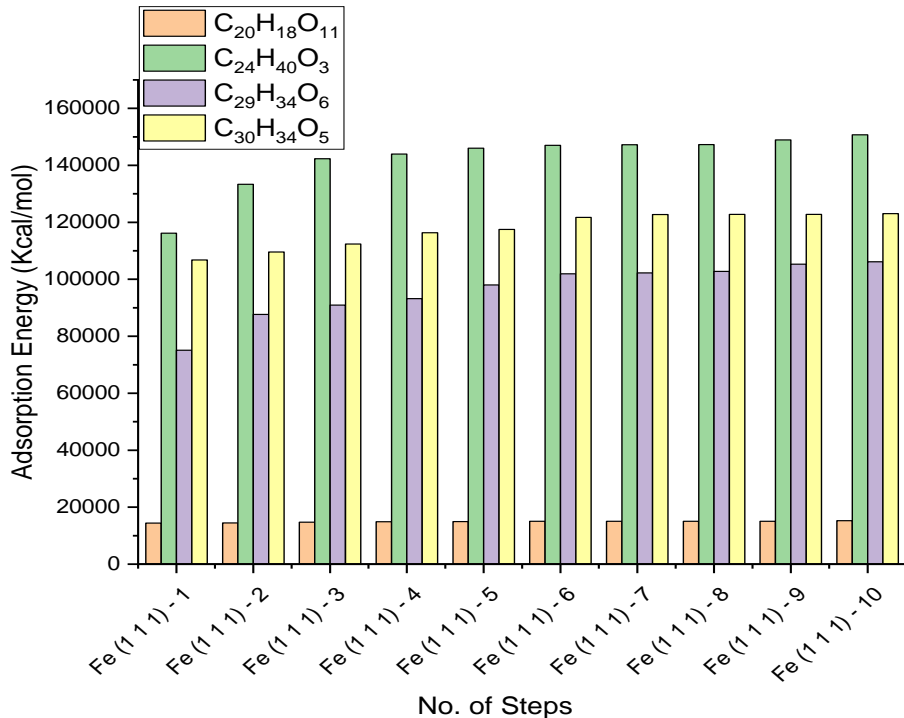


Figure 7. Adsorption energies relevant to each simulation step on the surface of Fe (111) crystal

4.2. Density function theory (DFT) and chemical descriptors

Computation conducted with Spartan “14V1.1.4” software using density functional theory (DFT) with the Becke’s three-parameter exchange functional (B3) along with the Lee-Yang-Parr (LYP) gradient corrected nonlocal correlation functional (B3LYP) at 6-311+G** and 6-31G** basis sets in both gas and aqueous phase respectively [9,17,19,21,25]. DFT calculations are widely implemented in computational chemistry due to the reliability and compatibility of its predictions with the experimental data [18]. Moreover, B3LYP has been assigned for systems comprising transition metal atoms during corrosion inhibition study, since the inhibitor adsorption on the metallic layer depends on donor-acceptor interaction between the vacant d-orbital of the metal atoms and the conjugated π -electrons of the heterocyclic atom [18]. The input files were built with ChemBioDraw, then the geometry of the neutral molecule equilibrated using DFT- B3LYP at the same basis sets in the gas and water phase. The relation of the quantum chemical descriptors to the corrosion inhibition behavior of the reported inhibitors was investigated [19]. These descriptors include Frontier molecular orbitals (FMO) energies (E_{HOMO} & E_{LUMO}); Ionization potential (I); Electron affinity (A); The energy bandgap ($\Delta E_{LUMO-HOMO}$); Absolute electronegativity (χ); Global hardness (η); Global softness (σ); Global electrophilicity index (ω); Nucleophilicity (ε); Electronic chemical potential (μ); The dipole moment (ψ); The fraction of electron transferred (ΔN); and $\Delta E_{Back-donation}$ (Total energy change, ΔTE) [11,17,19-21,23,25]. The detailed explanation of these descriptors with their empirical formula are provided in supporting information for further readings. The optimized geometries as well as Frontier molecule orbital (HOMO & LUMO) delocalization, and electrostatic potential map (ESP) of the reported inhibitor molecules in the aqueous and gas phases are shown in Figures 8 & 9 respectively. Chemical descriptors calculated by DFT- method in both gas and aqueous phase are summarized in Table 6.

Table 6. Chemical descriptors of the reported inhibitors in gas and aqueous phase

Chemical de-scriptors	Gas-phase (6-311+G**)				The aqueous phase (6-31G**)			
	C₂₀	C₂₄	C₂₉	C₃₀	C₂₀	C₂₄	C₂₉	C₃₀
E_{HOMO} , eV	-6.4100	-6.3700	-6.6600	-6.5200	-8.2200	-5.8700	-6.1000	-6.1200
E_{LUMO} , eV	-2.4700	-2.1700	-2.3600	-2.1400	-1.8200	-1.8100	-1.7100	-1.6500
ψ , Debye	5.9800	4.1800	4.2500	7.0800	7.0700	5.2400	4.6300	8.3800
I , eV	6.4100	6.3700	6.6600	6.5200	8.2200	5.8700	6.1000	6.1200
A , eV	2.4700	2.1700	2.3600	2.1400	1.8200	1.8100	1.7100	1.6500
ΔE_{gap} , eV	3.9400	4.2000	4.3000	4.3800	6.4000	4.0600	4.3900	4.4700
χ	4.4400	4.2700	4.5100	4.3300	5.0200	3.8400	3.9050	3.8850
η , eV	1.9700	2.1000	2.1500	2.1900	3.2000	2.0300	2.1950	2.2350
σ , eV ⁻¹	0.5076	0.4762	0.4651	0.4566	0.3125	0.4926	0.4556	0.4474
μ	-4.4400	-4.2700	-4.5100	-4.3300	-5.0200	-3.8400	-3.9050	-3.8850
ω , eV	5.0035	4.3412	4.7303	4.2806	3.9376	3.6319	3.4736	3.3766
ε	0.1998	0.2303	0.2114	0.2336	0.2539	0.2753	0.2878	0.2961
ΔN	0.6497	0.6500	0.5791	0.6096	0.3094	0.7783	0.7050	0.6969
$\Delta E_{Back-donation}$, eV	-0.4925	-0.5250	-0.5375	-0.5475	-0.8000	-0.5075	-0.5488	-0.5588

The molecular distribution of the LUMO and HOMO orbitals in the gas and aqueous phases displayed in Figures 8 & 9. They are mainly concentrated on the hetero (O) atoms and aromatic rings containing hetero (O) atoms in the four structures. This means that the aromatic rings and hetero oxygen atoms are mainly engaged in the electrons sharing through metal inhibitor interactions. The molecular electrostatic potential (ESP) map has been characterized by different colors which indicate the electron density distribution through the whole molecule [21]. Red colors assigned for negative electrostatic potential, while blue regions correspond to positive ones [9].

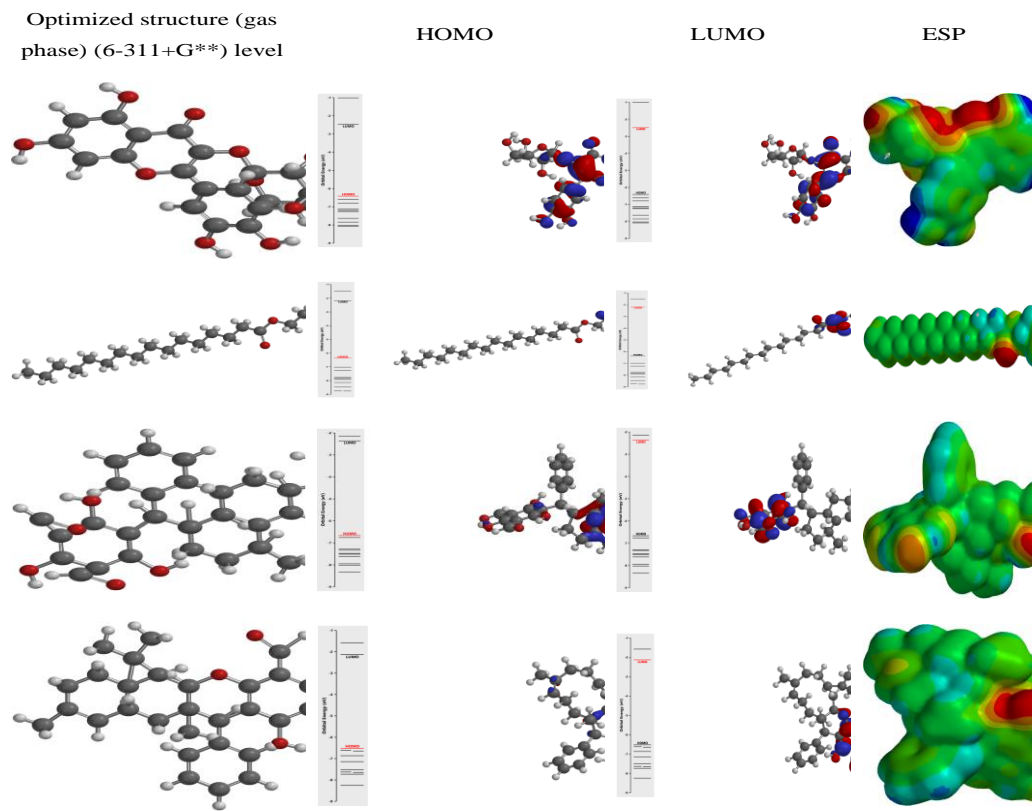


Figure 8. Optimized geometries, HOMO, LUMO, and ESP in the gas phase

($\ddot{\text{O}}$) atoms of the aromatic and furan rings contain lone pair of electrons, so have the most negative charges (red regions). Consequently, ($\ddot{\text{O}}$) atoms are the negatively charged sites that give electrons to the Fe metal forming coordinate bond [12]. The hydroxyl groups (-OH) (dark blue regions) have more positive charges. The green regions assigned for neutral or zero electrostatic potential of the alkyl groups [9,21]. The HOMO levels stabilization in the gas phase and aqueous solution of the screened structures indicates their ability to give electrons to the metallic surface. The LUMO levels of the four inhibitors (in their gaseous and aqueous phases reveal similar observation [9]). The insignificant energy discrepancy between the LUMO levels for the four inhibitors reveals an equal tendency to pull out electrons from the metal (Fe) surface to their LUMO orbitals [9]. By analyzing the chemical descriptors in the aqueous phase as displayed in Table 6, the E_{HOMO} increases in the aqueous phase in the following order; $\text{C}_{20}\text{H}_{18}\text{O}_{11} < \text{C}_{30}\text{H}_{34}\text{O}_5 < \text{C}_{29}\text{H}_{34}\text{O}_6 < \text{C}_{24}\text{H}_{40}\text{O}_3$. The highest value of E_{HOMO} (-6.37 eV) in the case of $\text{C}_{24}\text{H}_{40}\text{O}_3$ indicates its greater inhibition competence owing to the higher electron-donation ability from the molecule to the Fe surface. The lower the E_{LUMO} , the easier is the electrons acceptance from the (d) orbital of the Fe metal [19]. The lower energy gap ($\Delta E_{\text{LUMO-HOMO}}$) values indicate a good inhibition efficiency and relative chemical reactivity of Guajava leaf extract towards the metallic surface, owing to the lower energy needed to remove the electron from the HOMO orbital [12]. The reported ΔE values in Table 6 indicate that $\text{C}_{24}\text{H}_{40}\text{O}_3$ has the lowest ΔE values=4.06 eV, so it is expected to be the most efficient inhibitory molecule [19]. The lower ionization energy (5.87 eV) of the $\text{C}_{24}\text{H}_{40}\text{O}_3$ molecules confirms its higher inhibition efficiency [9,22]. By screening the global softness and hardness values, $\text{C}_{24}\text{H}_{40}\text{O}_3$ exhibit the highest global softness (0.4926 eV) and the lowest global hardness (2.03 eV) compared to other structures so, it is pronounced to be an efficient corrosion inhibitor rather than other components of Guajava leaf extract [24]. This assumption is based on the Lewis acid-base theorem which states that the metal (Fe) surface will interact with softer molecules faster than the harder molecules [9].

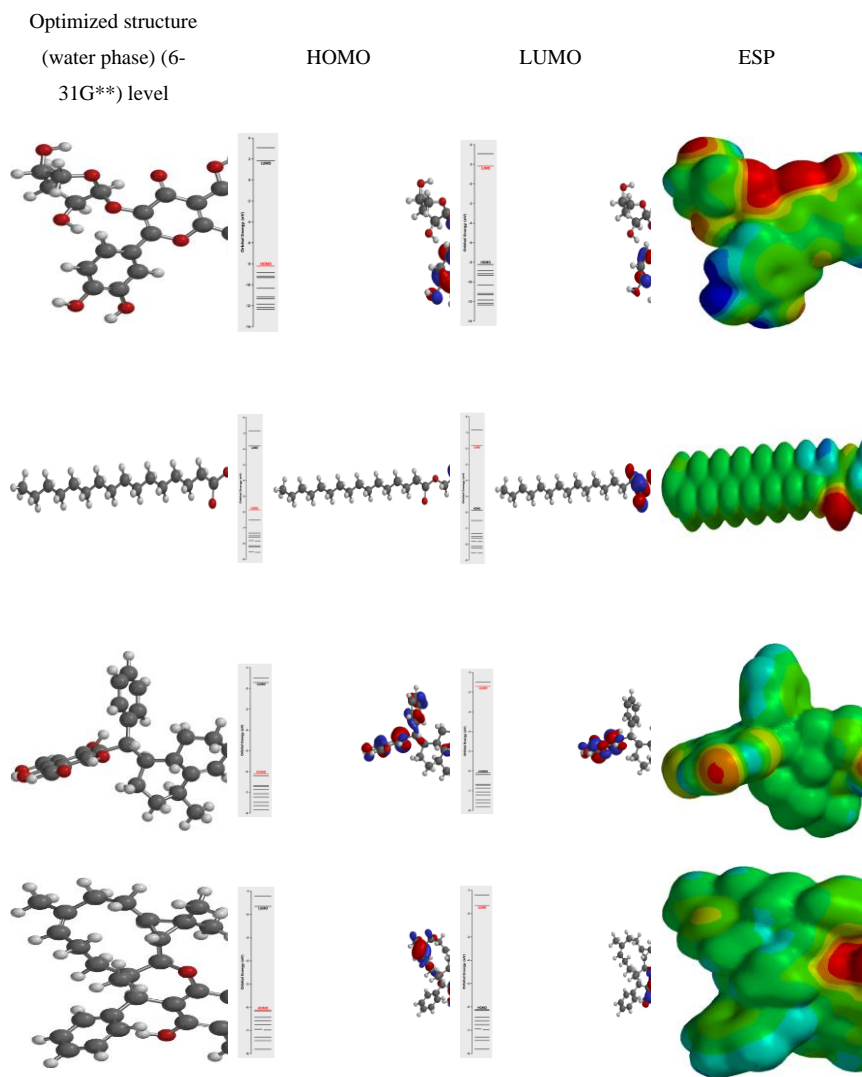


Figure 9. Optimized geometries, HOMO, LUMO, and ESP in the aqueous phase

Based on the electronegativity equalization principle of Sanderson [10-41], the lower electronegativity value of $C_{24}H_{40}O_3$ (3.84) ascertains its higher inhibition efficiency [24]. The results of electrophilicity as shown in Table 6 indicates that reactive, and efficient nucleophile is characterized by a low value of electronic chemical potential (μ) and electrophilicity index (ω) [19]. The fraction of electron transferred (ΔN) value exhibited that $C_{24}H_{40}O_3$ has a higher value of electron transfer (0.7783) so it exerts high inhibition effectiveness attributed to higher electron donating ability to the metallic surface based on Lukovits's study [19,42]. The electron flows from the molecule orbitals to the Fe metal till the chemical equilibrium is attained. Furthermore, the other inhibitors have $\Delta N > 0$, which indicates their capability to donate the electrons to the metal (Fe) surface [9]. $\Delta E_{\text{Back-donation}}$ calculated relevant to the global hardness, and revealed that back-donation is preferred for $C_{24}H_{40}O_3$ as good inhibitor [24]. Since $\Delta E_{\text{Back-donation}} < 0$, so the electron-back-donation process is energetically favored, and the inhibitor adsorption on the Fe surface is strengthened [9]. Although dipole moment (ψ) characterize the relative inhibitor reactivity towards the metallic surface. In this study the dipole moment has irregular trend. The efficiency of $C_{24}H_{40}O_3$ for corrosion inhibition resort to presence of several oxygen heteroatoms with plentiful n -electrons so adsorb effectively on the metallic

surface and resist the corrosive action [9,17]. The polar heteroatoms energize the inhibitor-metal cation adsorption interaction [9]. As a result, active binding sites on the Fe surface are congested, so, the anodic/cathodic interactions reduced during the electrochemical process [9]. Although the inhibition effectiveness improved with increasing the aliphatic chains [9,43], the presence of heteroatoms and conjugated π -electrons of the phenyl rings enhances the corrosion inhibition proficiency of $C_{20}H_{18}O_{11} < C_{30}H_{34}O_5 < C_{29}H_{34}O_6$ [17].

5. Conclusion

Psidium guajava extract comprises a mixture of inhibitors. The adsorption of *Psidium guajava*_extract obeys Langmuir adsorption isotherm. The increasing value of the CPE exponent reveals that surface roughness diminished with increasing the inhibitor concentration. Quantum chemical parameters including Frontier HOMO and LUMO molecular orbitals (E_{LUMO} , E_{HOMO}), chemical hardness, energy gap ($\Delta E_{LUMO-HOMO}$), electronegativity, and softness provide significant evidence about corrosion inhibition proficiency. The chemical descriptors have been computed using the DFT theorem with the B3LYP correlation functional method at 6-311+G** and 6-31G** basis sets in both gas and aqueous phase. Also, the molecular dynamic approach was conducted through the MC simulation. The adsorption energies of the reported inhibitors on the Fe surface (111)/H₂O interface were investigated. The results of molecular dynamics calculations show that the C₂₄H₄₀O₃ inhibitor gives the maximum adsorption energy. Consequently, C₂₄H₄₀O₃ performs greater inhibition efficiency as compared to other inhibitor molecules in the *Psidium guajava*_leaf extract. On the same side, the chemical descriptors outputs obtained from the DFT approach provides good insight into the inhibition performance of C₂₄H₄₀O₃ which is in great compliance with the results obtained from the Monte Carlo simulation.

Declaration of competing interests

The authors declare that they have no known competing for financial interests or personal relationships that could have appeared to influence the work reported in this paper.

References

- [1] Da Rocha JC, Gomes JAdCP, D'Elia E. Corrosion inhibition of carbon steel in hydrochloric acid solution by fruit peel aqueous extracts. *Corros Sci.*, 2010; 52(7):2341-8.
- [2] Cang H, Fei Z, Shao J, Shi W, Xu Q. Corrosion inhibition of mild steel by aloes extract in HCl solution medium. *International Journal of Electrochemical Science*, 2013; 8(1): 720-34.
- [3] Buchweishaija J, Mhinzi G. Natural products as a source of environmentally friendly corrosion inhibitors: the case of gum exudate from *Acacia seyal* var. *seyal*. *Portugaliae Electrochimica Acta*, 2008; 26(3): 257-65.
- [4] Oguzie EE. Evaluation of the inhibitive effect of some plant extracts on the acid corrosion of mild steel. *Corros Sci.*, 2008; 50(11): 2993-8.
- [5] Soltani N, Tavakkoli N, Khayatkashani M, Jalali MR, Mosavizade A. Green approach to corrosion inhibition of 304 stainless steel in hydrochloric acid solution by the extract of *Salvia officinalis* leaves. *Corros Sci.*, 2012; 62: 122-35.
- [6] Valek L, Martinez S. Copper corrosion inhibition by *Azadirachta indica* leaves extract in 0.5 M sulphuric acid. *Mater Lett.*, 2007; 61(1): 148-51.
- [7] Avwiri GO, Igho F. Inhibitive action of *Vernonia amygdalina* on the corrosion of aluminium alloys in acidic media. *Mater Lett.*, 2003; 57(22-23): 3705-11.
- [8] Orubite-Okorosaye K, Oforka N. Corrosion inhibition of zinc on HCl using *Nypa fruticans* Wurmb extract and 1, 5 diphenyl carbazonen. *Journal of Applied Sciences and Environmental Management*, 2004; 8(1): 56-61.
- [9] Obot I, Onyeachu IB, Wazzan N, Al-Amri AH. Theoretical and experimental investigation of two alkyl carboxylates as corrosion inhibitors for steel in acidic medium. *J Mol Liq.*, 2019; 279: 190-207.
- [10] El-hoshoudy A, Soliman F, Mansour E, Zaki T, Desouky S. Experimental and theoretical investigation of quaternary ammonium-based deep eutectic solvent for secondary water flooding. *J Mol Liq.*, 2019; 294: 111621.
- [11] Negm N, Migahed M, Farag R, Fadda A, Awad M, Shaban M. High performance corrosion inhibition of novel tricationic surfactants on carbon steel in formation water: Electrochemical and computational evaluations. *J Mol Liq.*, 2018; 262: 363-75.

- [12] Musa AY, Jalgham RT, Mohamad AB. Molecular dynamic and quantum chemical calculations for phthalazine derivatives as corrosion inhibitors of mild steel in 1 M HCl. *Corros Sci.*, 2012; 56: 176-83.
- [13] El-hoshoudy A, Mansour E, Desouky S. Experimental, computational and simulation oversight of silica-co-poly acrylates composite prepared by surfactant-stabilized emulsion for polymer flooding in unconsolidated sandstone reservoirs. *J Mol Liq.*, 2020; 113082.
- [14] El-hoshoudy A, Zaki E, Elsaed S. Experimental and Monte Carlo simulation of palmitate-guar gum derivative as a novel flooding agent in the underground reservoir. *J Mol Liq.*, 2020; 112502.
- [15] El-hoshoudy A, Soliman F, Abd El-Aty DM. Extractive desulfurization using choline chloride-based DES/molybdate nanofluids; Experimental and theoretical investigation. *J Mol Liq.*, 2020; 318: 114307.
- [16] El-hoshoudy A, Zaki E, Elsaed S. Experimental and Monte Carlo simulation of palmitate-guar gum derivative as a novel flooding agent in the underground reservoir. *J Mol Liq.*, 2020; 302: 112502.
- [17] Dagdag O, Safi Z, Erramli H, Wazzan N, Obot I, Akpan E, et al. Anticorrosive property of heterocyclic based epoxy resins on carbon steel corrosion in acidic medium: Electrochemical, surface morphology, DFT and Monte Carlo simulation studies. *J Mol Liq.*, 2019; 110977.
- [18] Wang H, Wang X, Wang H, Wang L, Liu A. DFT study of new bipyrazole derivatives and their potential activity as corrosion inhibitors. *J Mol Model.* 2007; 13(1): 147-53.
- [19] Gad EA, Al-Fahemi JH. Adsorptivity and corrosion inhibition performance of 2-(alkyloxy)-N, N, N-tris (2-hydroxyethyl)-2-oxo-ethanaminium chloride using DFT Approach. *Int J Sci Eng Res.*, 2015 ;6(10): 570-6.
- [20] Al-Fahemi JH, Abdallah M, Gad EA, Jahdaly B. Experimental and theoretical approach studies for melatonin drug as safely corrosion inhibitors for carbon steel using DFT. *J Mol Liq.*, 2016; 222: 1157-63.
- [21] Kaya S, Tütün B, Kaya C, Obot IB. Determination of corrosion inhibition effects of amino acids: quantum chemical and molecular dynamic simulation study. *Journal of the Taiwan Institute of Chemical Engineers* 2016; 58: 528-35.
- [22] Gad EA, Azzam E, Halim SA. Theoretical approach for the performance of 4-mercaptop-1-alkylpyridin-1-iun bromide as corrosion inhibitors using DFT. *Egyptian Journal of Petroleum*, 2018; 27(4): 695-699.
- [23] Verma C, Quraishi M, Ebenso EE, Bahadur I. A green and sustainable approach for mild steel acidic corrosion inhibition using leaves extract: experimental and DFT studies. *Journal of Bio- and Tribro-Corrosion*, 2018; 4(3): 33.
- [24] Abdallah M, Gad EA, Al-Fahemi JH, Sobhi M. Experimental and Theoretical Investigation by DFT on the Some Azole Antifungal Drugs as Green Corrosion Inhibitors for Aluminum in 1.0 M HCl. *Protection of Metals and Physical Chemistry of Surfaces*, 2018; 54(3): 503-12.
- [25] Bedair M, Soliman S, Hegazy M, Obot I, Ahmed A. Empirical and theoretical investigations on the corrosion inhibition characteristics of mild steel by three new Schiff base derivatives. *J Adhes Sci Technol.*, 2019; 33(11): 1139-68.
- [26] Anupama K, Abraham J. Electroanalytical studies on the corrosion inhibition behavior of guava (*Psidium guajava*) leaves extract on mild steel in hydrochloric acid. *Res Chem Intermed*, 2013; 39(9): 4067-80.
- [27] Victoria SN, Prasad R, Manivannan R. *Psidium guajava* leaf extract as green corrosion inhibitor for mild steel in phosphoric acid. *Int J Electrochem Sci.*, 2015; 10: 2220-38.
- [28] Fouad A, Shalabi K, E-Hossiany A. Moxifloxacin antibiotic as green corrosion inhibitor for carbon steel in 1 M HCl. *Journal of Bio- and Tribro-Corrosion*, 2016; 2(3): 18.
- [29] Migahed M, Zaki E, Shaban M. Corrosion control in the tubing steel of oil wells during matrix acidizing operations. *RSC advances*, 2016; 6(75): 71384-96.
- [30] Bentiss F, Bouanis M, Mernari B, Traisnel M, Vezin H, Lagrenée M. Understanding the adsorption of 4H-1, 2, 4-triazole derivatives on mild steel surface in molar hydrochloric acid. *Appl Surf Sci.*, 2007; 253(7): 3696-704.
- [31] El-Sabbah M, Bedair MA, Abbas MA, Fahmy A, Hassaballa S, Moustafa AA. Synergistic Effect between Natural Honey and 0.1 M KI as Green Corrosion Inhibitor for Steel in Acid Medium. *Z Phys Chem.*, 2019; 233(5): 627-49.
- [32] Elsaed S, El Sayed H, Ashour H, Zaki E, Khamis E, El Nagy H. Corrosion and hydrogen evolution rate control for X-65 carbon steel based on chitosan polymeric ionic liquids: experimental and quantum chemical studies. *RSC advances*, 2018; 8(66): 37891-904.

- [33] Soliman S, Metwally M, Selim S, Bedair M, Abbas MA. Corrosion inhibition and adsorption behavior of new Schiff base surfactant on steel in acidic environment: Experimental and theoretical studies. *Journal of Industrial and Engineering Chemistry*, 2014; 20(6): 4311-20.
- [34] Abd-Elaal AA, Elbasiony N, Shaban SM, Zaki E. Studying the corrosion inhibition of some prepared nonionic surfactants based on 3-(4-hydroxyphenyl) propanoic acid and estimating the influence of silver nanoparticles on the surface parameters. *J Mol Liq.*, 2018; 249: 304-17.
- [35] Ismail AS, Abbas MA. The Corrosion Performance of Al-Si and Al-Cu Casting Alloys in H₂SO₄ and Na₂CO₃ Media. *Silicon*, 2017; 9(2): 193-9.
- [36] Singh D, Chaudhary R, Prakash B, Agarwal C. Inhibitive efficiency of some substituted thioureas for the corrosion of aluminium in nitric acid. *Br Corros J.*, 1979; 14(4): 235-9.
- [37] El-hoshoody AN, Ghanem A, Desouky SM. Imidazolium-based ionic liquids for asphaltene dispersion; experimental and computational studies. *J Mol Liq.*, 2020; 114698.
- [38] Khaled K. Experimental and molecular dynamics study on the inhibition performance of some nitrogen containing compounds for iron corrosion. *Mater Chem Phys.*, 2010; 124(1): 760-7.
- [39] Khaled K. Electrochemical behavior of nickel in nitric acid and its corrosion inhibition using some thiosemicarbazone derivatives. *Electrochim Acta*, 2010; 55(19): 5375-83.
- [40] Sanderson RT. Electronegativity and bond energy. *J Am Chem Soc.*, 1983; 105(8): 2259-61.
- [41] Bratsch SG. Electronegativity equalization with Pauling units. *J Chem Educ.*, 1984; 61(7): 588.
- [42] Lukovits I, Kalman E, Zucchi F. Corrosion inhibitors—correlation between electronic structure and efficiency. *Corrosion*, 2001; 57(1): 3-8.
- [43] Dinodi N, Shetty AN. Alkyl carboxylates as efficient and green inhibitors of magnesium alloy ZE41 corrosion in aqueous salt solution. *Corros Sci.*, 2014; 85: 411-27.

To whom correspondence should be addressed: Dr. A. N. El-hoshoody, Egyptian Petroleum Research Institute, 11727, Nasr City, Cairo, Egypt, E-mail: azizchemist@yahoo.com